Front-Side-Illuminated InGaAs/InP Modified UTC-Photodiodes With Cliff Layer

Wenjun Li [a], Andreas Beling [b], Joe Campbell [b], Glen Hillier [c],
Chris Stender [c], Noren Pan [c], and Patrick Fay [a*]

a) Department of Electrical Engineering, University of Notre Dame, Notre Dame, IN, 46556
b) Department of Electrical and Computer Engineering, University of Virginia, Charlottesville, VA, 22904
c) MicroLink Devices, Inc., Niles, IL, 60714
* Tel: (574) 631-5693, Email: pfay@nd.edu

Keywords: Photodiode, III-V Fabrication

5

Abstract

Fabrication and characterization of a front-side illuminated InGaAs/InP modified uni-travelling-carrier photodiode (MUTC-PD) with cliff layer has been demonstrated experimentally. The resulting photodiodes exhibit a low dark current density of 1.30×10^{-2} A/cm^2 at -5 V, and a measured responsivity of 0.24 A/W at 1.55 µm (without antireflection coating). Inclusion of an anti-reflection coating could enhance the responsivity to 0.36 A/W. Under low-level illumination conditions, a 27 µm diameter device exhibits a measured small-signal bandwidth of 8.8 GHz. Contrary to conventional p-i-n photodiodes, the bandwidth of the MUTC-PD is shown to increase with increasing input optical power; the devices shown here have bandwidths of 12.8 GHz at an optical intensity of 14.1 µW/µm^2.

INTRODUCTION

In many advanced microwave applications, such as phased array radar, microwave signal processing, wireless communication, and others [1]-[3], optical fiber is an attractive alternative to the use of coaxial cable as the media to transmit the microwave signal within the system, due to its advantages in terms of low loss, wide bandwidth transmission, and light weight [4]. Compared to all-electronic approaches, these hybrid optical/microwave systems can potentially offer reduced size, lower cost, lower attenuation and higher transmission capacity [4]. In a typical microwave photonic link, the microwave electrical signal is converted into an optical signal at the transmitting side, transported over optical fiber, and then converted back into an electrical signal at the receiving end [5]. Two important figures of merit for microwave photonic links of this type are insertion loss and dynamic range. To improve the microwave optical link performance, it is crucial to increase the electrical/optical and optical/electrical conversion efficiencies to reduce link insertion loss, and to suppress system nonlinearities to improve dynamic range. By using photodiodes with high power handling capability and high linearity, the signal efficiency and dynamic range performance of the receiver can be greatly enhanced [6].

The two main factors that limit the high-power behavior of photodiodes are space charge effects and thermal runaway [7]. While thermal effects can typically be reduced by thermal management strategies [8], space charge effects mainly depend on the intrinsic physics of the device design [7]. Compared with conventional p-i-n photodiodes, uni-travelling-carrier photodiodes (UTC-PDs) can effectively suppress space-charge effects and increase the output current, by designing the structure so that only electrons contribute to the external photocurrent [9]. Because of the superior transport properties of electrons relative to holes in typical III-V materials, UTC-PDs can also have a higher transit-time limited bandwidth than comparable p-i-n photodiodes. The UTC-PD bandwidth and output power performance can be further enhanced by insertion of both an undoped optical absorption layer to increase responsivity [10, 11] and a charge-compensation layer to tailor the internal electric field profile [12, 13], resulting in a modified UTC-PD (MUTC-PD) with cliff layer [13].

FABRICATION

The heterostructure used to fabricate the InGaAs/InP MUTC-PDs reported here was grown on a semi-insulating InP substrate by metalorganic chemical vapor deposition (MOCVD). As shown in Fig. 1(a), the heterostructure consists of a 50 nm p-type $GaAs_{0.5}Sb_{0.5}$ anode contact layer followed by a 100 nm heavily doped p-type InP carrier blocking layer to prevent photogenerated electrons from entering the anode contact. Compared with traditional use of InGaAs as the anode contact layer, the use of GaAsSb provides a more favorable energy band alignment [13]. The incident light is absorbed in both a 700 nm thick p-type $In_{0.53}Ga_{0.47}As$ absorption layer and a 150 nm thick lightly n-doped $In_{0.53}Ga_{0.47}As$ absorption layer. The doping level in the absorption region is graded in steps, in order to create a quasi-electric field to further promote electron transport. Unlike a conventional UTC-photodiode, which uses a uniformly-doped p-type $In_{0.53}Ga_{0.47}As$ layer for optical absorption, the insertion of an undoped or lightly n-doped layer as shown here can increase the photodiode efficiency-bandwidth product; the additional layer serves both to increase the light absorption layer thickness (increasing

responsivity), while at the same time enhancing carrier transport in the depleted absorption layer [10][11]. The lightly n-doped InGaAs layer also helps to compensate the space charge generated under high optical illumination levels. The photogenerated electrons exit the absorption layer and are collected using a 50 nm InP cliff layer, 900 nm thick InP depletion layer, and 20 nm thick n-type $In_{0.53}Ga_{0.47}As$ cathode contact layer. The InP cliff layer serves to mitigate the space-charge effect at high photocurrent levels [12][13], and InGaAsP layers in the heterostructure are used to minimize the band discontinuities between $In_{0.53}Ga_{0.47}As$ and InP. Fig. 1(b) shows the calculated energy band diagram of this structure along the vertical direction, when the photodiode is not biased.

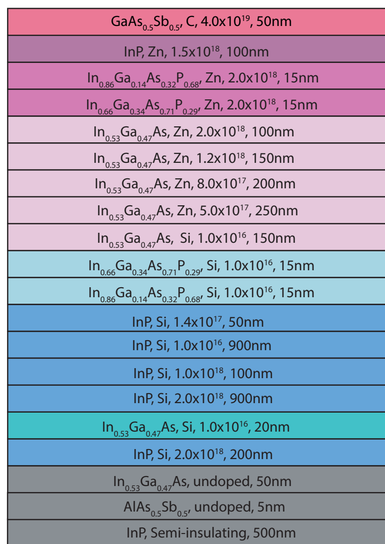

(a)

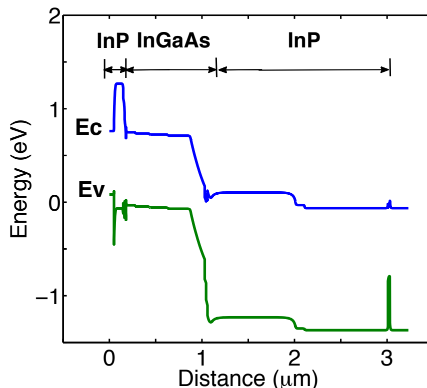

(b)

Fig. 1. (a) Schematic diagram of heterostructure for the InGaAs/InP MUTC-PD [13]; (b) Calculated energy band diagram.

A mesa-based fabrication process was used to fabricate the devices. In the process flow used for the devices reported here, anode contacts were first defined by electron-beam evaporation of Ti/Au. A series of selective wet chemical etches was then used to define the active region and the bottom contact mesa areas. For these etches, 4:1:50 $H_3PO_4/H_2O_3/H_2O$, 3:1 H_3PO_4/HCl, 1:1:10 $H_2SO_4/H_2O_3/H_2O$ and buffered HF solutions were used to etch GaAsSb, InGaAs, InP and AlAsSb, respectively (all ratios are volumetric). Cathode contacts were defined on the bottom n-type InGaAs layer with thermal evaporation of AuGe/Ni/Au, followed by a rapid thermal annealing at 300 $^{\circ}$C for 20 seconds in an argon ambient. After that, benzocyclobutene (BCB) was spun on for sidewall passivation, and vias in the BCB were opened by reactive ion etching (RIE) in SF_6/O_2 plasma. To enable on-wafer RF measurements, ground-signal-ground RF pads were deposited using electron-beam evaporation and lift-off. Finally, BCB was etched off in the optical window area. The schematic cross-section of the fabricated device is shown in Fig. 2.

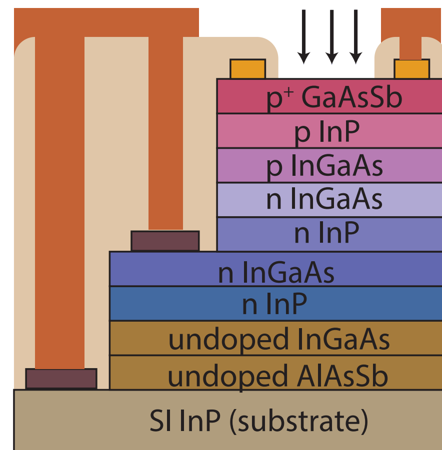

Fig. 2. Cross-sectional schematic of a front-side illuminated InGaAs/InP MUTC-PD.

MEASUREMENTS

Since the dark current is a key metric that sets the lower bound on noise performance of a photodetector, the dark current of the photodiodes was measured experimentally from 0 V to -5 V. At a reverse bias of 5 V, a typical dark current density of 1.30×10^{-2} A/cm^2 was obtained. By measuring devices with junction areas ranging from 152 to 1128 μm^2 (Fig. 3(a)), the dark current was found to scale nearly linearly with the junction area, as shown in Fig. 3 (b). The deviation of the experimental data from the fitted curve can be explained by the junction area reduction due to undercut during the wet etch processing. This result does suggest, however, that surface recombination in these structures (which would give rise to a perimeter-related dark current component) is not significant.

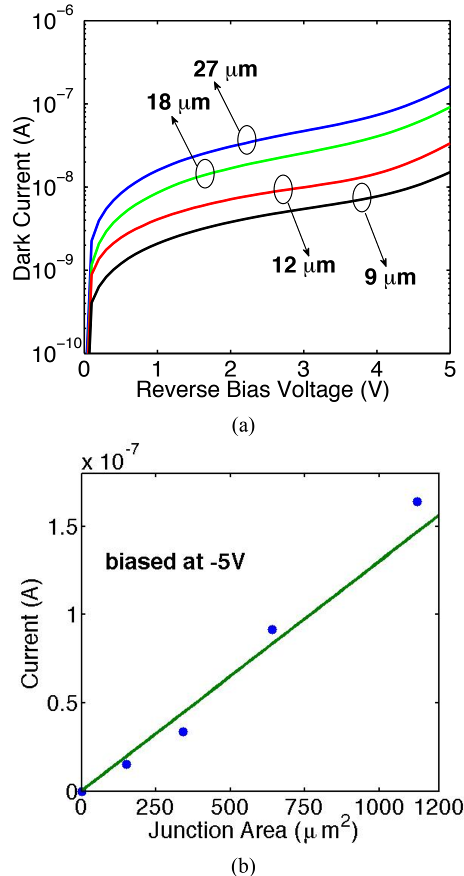

(a)

(b)

Fig. 3. (a) Dark current as a function of reverse bias for MUTC-PDs with different junction diameters, and (b) dependence of dark current on junction area at -5 V bias. The linear relationship between dark current and junction area suggests limited surface recombination is present in these devices.

The voltage dependence of the photodiode capacitance was also measured; as shown in Fig. 4, the devices are fully depleted at around -5 to -7 V. The capacitance measurements both provide a guide for selecting suitable bias conditions for RF measurements, as well as an estimate of the RC-limited bandwidth of the devices.

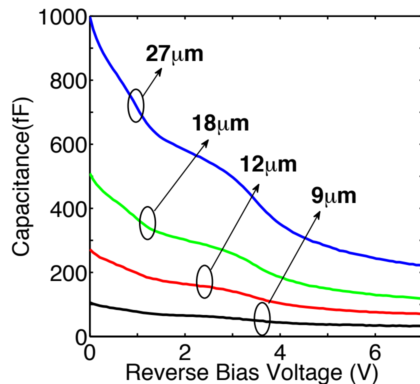

Fig. 4. Capacitance-voltage characteristics measured at 1 MHz for typical MUTC-PDs at different junction diameters.

The responsivity of the devices under DC illumination at 1550 nm was measured to be 0.24 A/W, without the use of an antireflection coating. Since the surface material $GaAs_{0.5}Sb_{0.5}$ produces a normal-incidence light reflectivity of ~33%, the inclusion of an anti-reflection coating could enhance the photodiode responsivity to as much as 0.36 A/W. In addition, the responsivity could be further enhanced by using a back-side illuminated structure with reflecting top anode contact, since in these structures the effective absorption length is doubled as a result of the two-pass optical path [13].

The high frequency characteristics of the devices were also assessed. Fig. 5(a) shows the experimental setup for frequency response measurement. 1550 nm light emitted from a distributed feedback laser diode was modulated by a Mach-Zehnder modulator. The DC bias of the modulator was adjusted to maximize the RF output using a reference detector, and the RF input was provided by a network analyzer. Due to its polarization-dependence, polarization maintaining fiber was used between the modulator and laser. After going through a variable optical attenuator to set the incident illumination level, the modulated light was focused on the device under test using a lensed single-mode fiber probe. Bias was supplied to the photodiode using an Agilent 4155C semiconductor parameter analyzer through the network analyzer's built-in bias tee. The alignment between the fiber probe and the device was made by maximizing the photodiode electrical output, while keeping the input optical power constant. After alignment, the frequency response of the photodiode was measured using the network analyzer. Effects of imperfections in the optical components and the electrical components were removed using a calibration procedure based on a high speed reference photodetector with known frequency response.

Fig. 5(b) shows the measured frequency response for a typical 27 μm-diameter photodiode when biased at -8 V, for two different optical illumination intensities. The 3 dB bandwidth of this 27 μm-diameter photodiode increases from 8.8 GHz to 12.8 GHz with an increase of optical illumination intensities from 0.07 $\mu W/\mu m^2$ to 14.1 $\mu W/\mu m^2$. This nonlinear bandwidth expansion arises because increased optical generation produces an increase in the internal electric field in the absorption region that accelerates the electrons (contrary to the case of conventional p-i-n photodiodes), which enhances the high-speed performance of the photodiode [14]. Fig. 5(c) shows the inverse area dependence of the 3 dB bandwidth, for an input optical illumination intensity of $0.07\mu W/\mu m^2$. The RC time constant, τ_{RC}, and carrier transit time, τ_{tr}, were extracted by curve fitting. The carrier transit time τ_{tr} was found to be 8.91

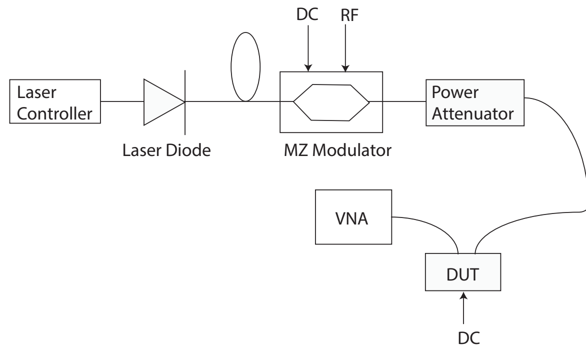

(a)

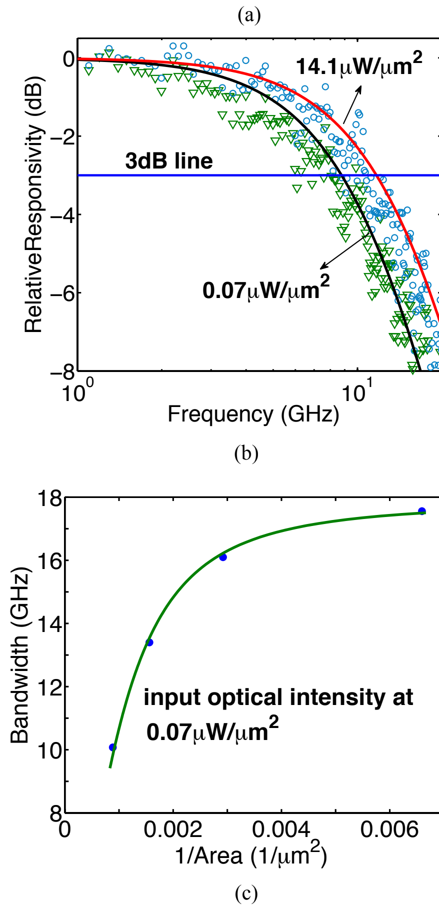

(b)

(c)

Fig. 5. (a) Diagram of the experimental setup for photodiode frequency response measurement; (b) measured frequency response for 27 μm-diameter device at different photocurrent levels, corresponding to optical illumination intensities of 0.07 $\mu W/\mu m^2$ and 14.1 $\mu W/\mu m^2$; (c) area dependence of the measured 3 dB bandwidth for 0.07 $\mu W/\mu m^2$ optical intensity.

ps, which includes the carrier diffusion time in the undepleted absorption layer as well as carrier drift time in the depletion region. This results in an effective velocity of 2.19×10^7 cm/s, consistent with expectations for transport in InP. The τ_{RC} was found to be 1.20 $\mu s/cm^2$. Since the load for these measurements was 50 Ω, the resulting capacitance can be estimated to be 2.39×10^{-8} F/cm^2, which agrees well with the capacitance measurements shown in Fig. 4 of 2.03×10^{-8} F/cm^2 at full depletion.

CONCLUSIONS

In this work, the fabrication process of a front-side illuminated InGaAs/InP modified UTC-PD with a cliff layer was described, and the electrical performance has been assessed. A measured bandwidth of 8.8 GHz for a 27 μm diameter device was obtained under low incident optical intensity, increasing to 12.8 GHz as the optical intensity was increased to 14.1 $\mu W/\mu m^2$. This suggests a possibility for using them for high-power and high-speed applications in the microwave range, although the linearity implications of the observed bandwidth expansion have not been fully explored. These devices appear promising for high-performance microwave/optical links in advanced RF systems.

REFERENCES

[1] W. Ng, et al., *The first demonstration of an optically steered microwave phased array antenna using true-time-delay*. IEEE J. Lightwave Technol. 9, pp.1124-1131, 1991.
[2] R. A. Minasian, *Photonic signal processing of microwave signals*, Microwave Theory and Techniques, IEEE Transactions on, 54.2, pp. 832-846, 2006.
[3] M. Y. W. Chia et al., *Radio over multimode fibre transmission for wireless LAN using VCSELs*. Electron. Lett. 39.15, pp. 1143–1144, 2003.
[4] J. Capmany et al., *Microwave photonics combines two worlds*. Nature Photonics 1.6, pp. 319-330, 2007.
[5] S. Lezekiel, *Microwave Photonics Devices and Applications*. Wiley IEEE Press, 2009.
[6] C. H. Cox III et al., *Microwave Theory and Techniques*, IEEE Transactions on 54, pp.906-920, 2006.
[7] K. Williams et al., *Design considerations for high-current photodetectors*, J. Lightwave Technol.17, pp.1443-1454, 1999.
[8] N. Li, et al. *High power photodiode wafer bonded to Si using Au with improved responsivity and output power*, IEEE photonics technology letters 18.21-24, pp. 2526-2528, 2006.
[9] T. Ishibashi et al., *Uni-traveling-carrier photodiodes*, Tech. Dig. Ultrafast Electronics and Optoelectronics 13, pp. 83-87, 1997.
[10] D. H. Jun et al., *Improved efficiency-bandwidth product of modified uni-traveling carrier photodiode structures using an undoped photo-absorption layer*, Jpn. J. Appl. Phys. 45, pp.3475-3478, 2006.
[11] D. H. Jun et al., *A modified UTC-PD having high speed and efficiency characteristics utilizing a frequency compensation*, Semiconductor Device Research Symposium, 2003 International. IEEE, pp. 86-88, 2003.
[12] N. Li et al., *High-saturation-current charge-compensated InGaAs-InP uni-traveling-carrier photodiode*, Photonics Technology Letters, IEEE 16, pp.864-866, 2004.
[13] Z. Li et al., *High-saturation-current modified uni-traveling-carrier photodiode with cliff layer*, Quantum Electronics, IEEE Journal of 46, pp.626-632, 2010.
[14] N. Shimizu et al., *Improved response of uni-traveling-carrier photodiodes by carrier injection*, Jpn. J. Appl. Phys. 37, pp.1424-1426, 1998.